Title	Pulsed laser induced silicidation on TiN-capped Co/Si bilayers
Author(s)	Chow, F. L.; Lee, Pooi See; Pey, Kin Leong; Tang, L. J.; Tung, Chih Hang; Wang, X. C.; Lim, G. C.
Citation	Chow, F. L., Lee, P. S., Pey, K. L., Tang, L. J., Tung, C. H., Wang, X. C., et al. (2006). Pulsed laser induced silicidation on TiN-capped Co/Si bilayers. Journal of Applied Physics, 99(4).
Date	2006
URL	http://hdl.handle.net/10220/8022
Rights	

Pulsed laser-induced silicidation on TiN-capped Co/Si bilayers

F. L. Chow
Chartered Semiconductor Manufacturing Ltd., Singapore 738406, Singapore

P. S. Lee[a)]
School of Materials Science and Engineering, Nanyang Technological University, Singapore 639798, Singapore

K. L. Pey[b)]
Microelectronics Centre, School of Electrical and Electronic Engineering, Nanyang Technological University, Singapore 639798, Singapore

L. J. Tang and C. H. Tung
Institute of Microelectronics, Science Park II, Singapore 117685, Singapore

X. C. Wang and G. C. Lim
Singapore Institute of Manufacturing Technology, 71 Nanyang Drive, Singapore 638075, Singapore

(Received 26 April 2005; accepted 3 January 2006; published online 17 February 2006)

This paper studies the effects of pulsed laser-induced annealing of TiN-capped Co/Si bilayers with and without preamorphized Si substrate. For a low fluence of 0.2 J/cm^2, nonstoichiometry Co silicide with triple-layered structure is formed. On the other hand, highly textured $CoSi_2$ grains in (111) direction are formed for a high fluence of 0.7 J/cm^2. The highly textured $CoSi_2$ layer is monocrystalline and fully coherent with the (111) plane of the Si substrate. However, it has a large amount of microstructural defects throughout the layer. Competitive growth mechanisms between crystallization of homogenous intermixed layer and the nucleation from the melt boundary are discussed. © *2006 American Institute of Physics*. [DOI: 10.1063/1.2171774]

INTRODUCTION

In advanced complementary metal-oxide silicon (CMOS) technologies, the self-aligned silicide (SALICIDE) has shown the capability of lowering the resistance of gate and source/drain regions and contact resistance, thus increasing the device performance, especially for shallow junction and short channel devices. $CoSi_2$ has been widely used for sub-0.25 μm CMOS technology due to its low resistivity, good thermal stability, and the absence of fine-line effect in narrow lines. However, the Co silicidation is sensitive to oxygen contamination at the metal/Si interface. Hence, capping layers such as Ti and TiN have been introduced to prevent oxidation. The TiN-capped Co/Si silicide has been reported to have a large process window in controlling the silicide lateral growth.[1] Besides, the gate resistance can be reduced even for a gate length of 0.065 μm for the TiN-capped Co salicide process.[2] Moreover, it has been reported that the TiN capping layer has improved the current driving capability of *p*-type metal-oxide semiconductor field-effect transistors (pMOSFETs) compared to Ti capping layer.[3]

As semiconductor device dimensions continue to decrease, the main challenge in the area of silicide formation involves decreasing the silicide thickness while maintaining low contact silicide sheet resistance and low junction leakage. When the silicide thickness reaches 30 nm and below for 0.13 μm devices, the second rapid thermal annealing (RTA) process window becomes narrower.[4] Above a certain thermal budget the silicide agglomerates, causing the sheet resistance to increase. However, a minimum thermal budget is required for the formation of a smooth silicide/Si interface while maintaining good junction leakage.[4] An approach employing laser thermal annealing (LTA) to form $CoSi_2$ is investigated in this work. LTA provides several advantages compared to RTA. The use of laser irradiation, which deposits most of its energy near the sample surface, allows the reaction temperature for silicide formation and growth to be attained in the localized region of the irradiation, without the need of heating the entire wafer.[5] In addition, the laser-induced melt depth can be used to control the silicide thickness[6] and possibly reducing lateral growth. In addition, the composition of the silicide layer can be tailored by varying the laser fluence.[7]

In this paper, the transformation of Co silicide microstructure in TiN/Co/Si system by single-pulsed laser annealing at low and high fluences will be discussed. The effects of laser-induced TiN/Co/Si system with preamorphization implantation (PAI) layer will be investigated. The preamorphization layer has shown to improve thermal stability of silicide formation on silicon and polysilicon using rapid thermal processing.[8] Issues such as lateral voids, dopant segregation, thermal agglomeration, and increase of resistance on narrow linewidth are suppressed by using the PAI technology. Liu *et al.* has achieved a well-controlled Ti silicide thickness and a smooth Ti silicide/Si interface without ag-

[a)]Electronic mail: pslee@ntu.edu.sg
[b)]Electronic mail: eklpey@ntu.edu.sg

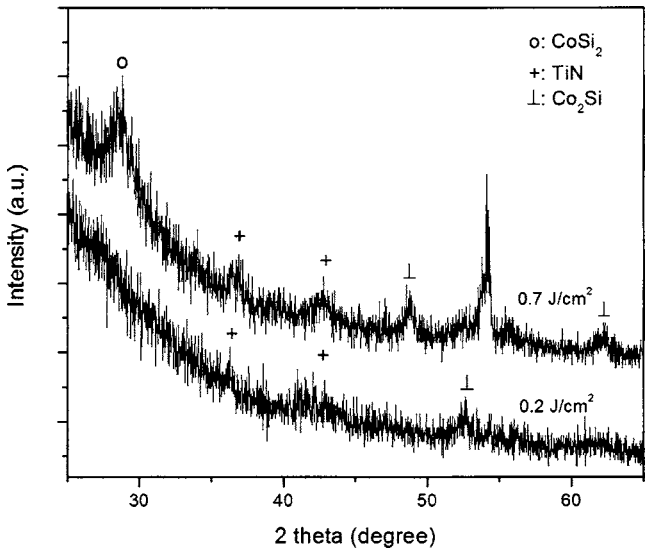

FIG. 1. Grazing incidence XRD spectra of a TiN/Co/Si system with PAI annealed for single pulse excimer laser at 0.2 and 0.7 J/cm^2.

glomeration using germanium preamorphization.[9] The PAI layer can also be utilized to control the melt depth for laser annealing for junction formation.[10]

EXPERIMENT

The starting material was an *n*-type (100) silicon wafer. Two types of samples were prepared. One of them was implanted with Si^+ at 20 keV to a dose of 2×10^{15} cm^{-2} in order to form a 50 nm preamorphization layer. Prior to metal deposition, the samples were subjected to a standard Radio Corporation of America (RCA) cleaning and followed by a diluted hydrofluoric acid clean. A 13 nm Co was deposited, followed by the deposition of a 20 nm TiN using dc magnetron sputtering without breaking vacuum. The samples were then irradiated in normal ambient (class 100 cleanroom) with a 248 nm KrF laser. Single pulse with pulse duration of 23 ns and fluences of 0.2 and 0.7 J/cm^2 was irradiated on the samples. The laser spot size was about 3×3 mm^2.

The sheet resistance was measured using four-point probe. A grazing incidence x-ray diffraction with an incident angle of 1° was used to identify the phase transformation after LTA. Auger electron spectroscopy (AES) was used to investigate the depth profile of silicide after LTA. The microstructures and thickness of the $CoSi_2$ were observed for some selected samples with cross-section transmission electron microscopy (XTEM). Electron dispersive x-ray spectroscopy (EDX) and electron-energy-loss spectroscopy (EELS) analyses with TEM were used to determine the localized elemental composition. In addition, the surface morphology of the films was examined using atomic force microscope (AFM).

RESULTS

Figure 1 shows the XRD spectra of a TiN/Co/Si system with a 50 nm PAI layer after single-pulsed laser annealing with fluences of 0.2 and 0.7 J/cm^2. Co silicide (111) peak was detected for both fluences with the peak intensity at 0.7 J/cm^2 being stronger than at 0.2 J/cm^2. However, the Co

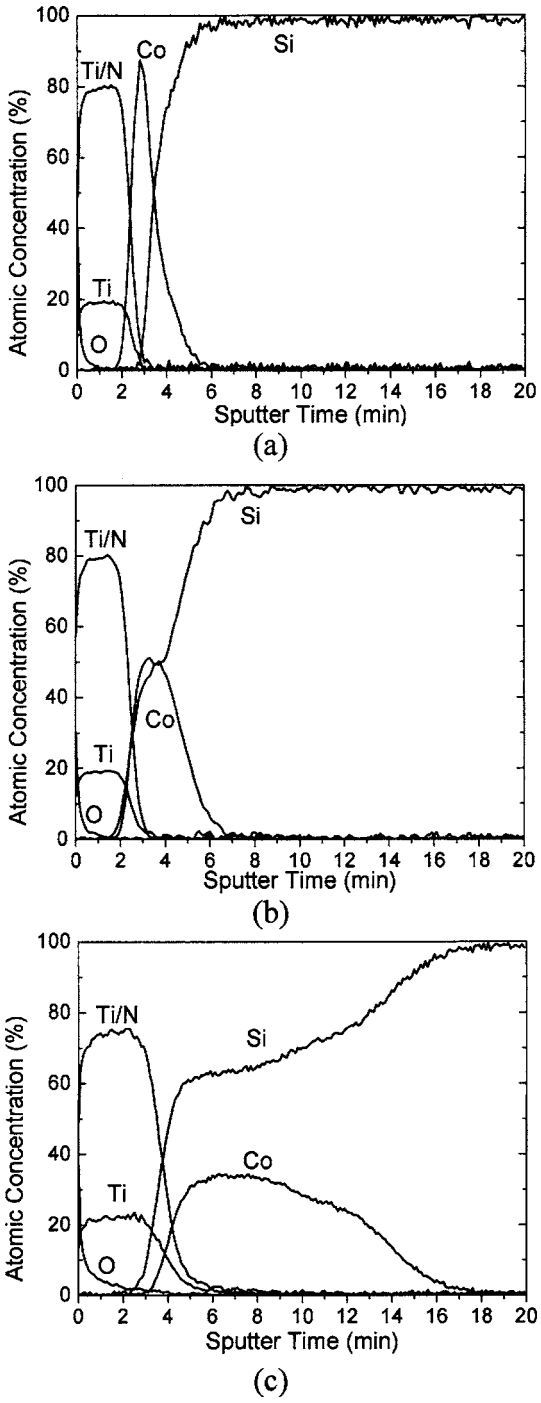

FIG. 2. AES depth profiles of the TiN/Co/Si systems with PAI (a) before annealing and after annealing with a single laser pulse at (b) 0.2 J/cm^2 and (c) 0.7 J/cm^2.

silicide peak intensity of 0.7 J/cm^2 is stronger than 0.2 J/cm^2. Co_2Si formation is observed for both 0.2 and 0.7 J/cm^2 samples. The XRD peaks at ~36.7° and ~42.6° correspond to the TiN (111) and (200) planes, respectively. Hence, this suggested that the capping layer stayed intact after the exposure to the high laser fluence. To examine the atomic distribution of the samples after LTA, AES was carried out for both fluences of 0.2 and 0.7 J/cm^2 for the TiN/Co/Si with PAI samples. The AES profile of the as-deposited sample before annealing is shown in Fig. 2(a) for comparison. The distribution of atomic concentration for

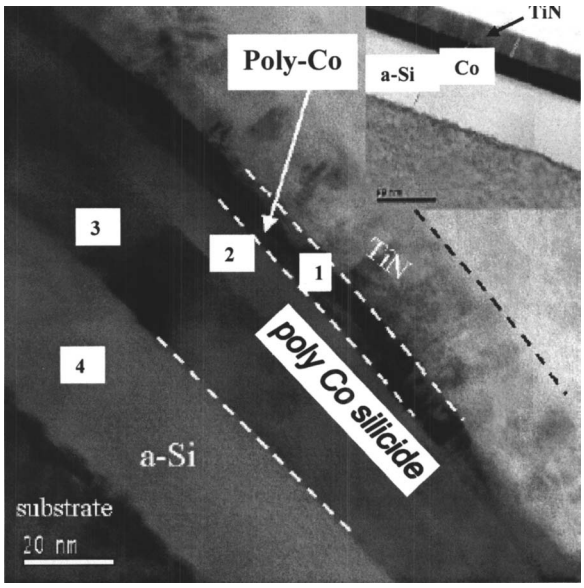

FIG. 3. XTEM image of the TiN/Co/Si system with PAI after single-pulsed laser irradiation at 0.2 J/cm^2. The inset shows the as-deposited TiN(20 nm)/Co(13 nm)/PAI(50 nm)/Si film stacks before annealing.

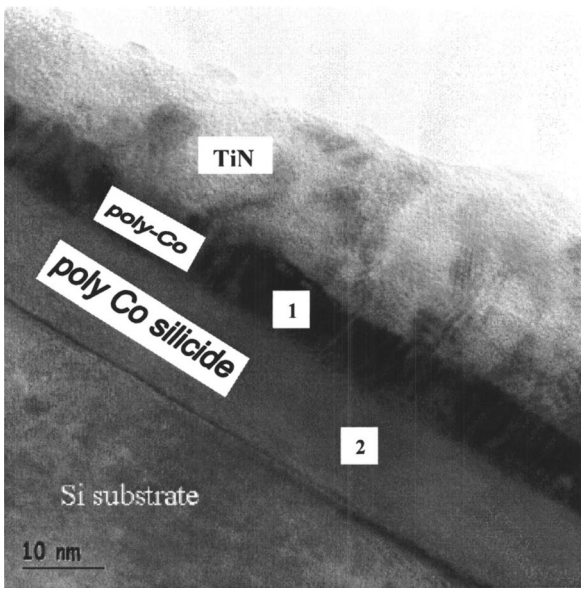

FIG. 4. XTEM image of the TiN/Co/Si system without PAI after single-pulsed laser irradiation at 0.2 J/cm^2.

single-pulsed LTA at 0.2 J/cm^2 is shown in Fig. 2(b). There is a minimal change in the depth profile and the TiN capping layer remains intact. Intermixing and interdiffusion of Co and Si have taken place. For the sample of 0.7 J/cm^2, as shown in Fig. 2(c), a larger extent of interdiffusion and intermixing of Co and Si has occurred for the PAI sample. Similar results were obtained for non-PAI substrates. A deeper melt depth was resulted in the 0.7 J/cm^2 samples compared to that of 0.2 J/cm^2. More Si atoms have taken part in the atomic interdiffusion in the liquid phase and a nearly 1:2 of Co:Si ratio has been achieved after solidification. Compared to the AES spectra of the 0.2 J/cm^2 sample, the depth profiling of the 0.7 J/cm^2 sample shows that TiN has propagated towards the substrate.

Figure 3 shows the microstructures of the TiN/Co/PAI-Si system after a single-pulsed laser annealing at 0.2 J/cm^2 while the inset shows the XTEM micrograph of an as-deposited sample. It can be seen that the 20 nm TiN layer stays intact but has deformed. A triple-layered microstructures can be observed (excluding the TiN and amorphous Si). The top layer which is in dark contrast is the unreacted polycrystalline Co of ~5.4 nm. The two bottom layers are the intermixed layer consisting of Co and Si atoms, and its total thickness is ~22 nm. The difference in the contrast in the poly-Co silicide layer indicates a difference in the compositional ratio and orientation of the Co silicide grains in the two layers. The elemental composition of the layer obtained by EDX/TEM analysis is shown in Table I. The upper layer is a 10 nm Co_2Si (as shown in XRD) and the other layer is of larger grained CoSi composition ratio. The random distribution of the grain structures in the poly-Co silicide layer indicates that crystallization has taken place after solidification.[11]

As shown in Fig. 4, on the contrary, the microstructures in the TiN/Co/Si system without PAI after single-pulsed laser annealing at 0.2 J/cm^2 are different from the system with PAI. A bilayered structure is clearly observed. The top layer is a poly-Co of ~8.3 nm and the bottom layer is an ~13 nm of poly-Co silicide. The corresponding TEM/EDX analysis and the estimated thickness of the layers are shown in Table I. The EDX detected insignificantly small amount of Ti in the top poly-Co layer for both systems. For the layers below the top unreacted Co layer, both systems give rise to poly-Co silicide that has almost similar atomic concentration distribution. Nevertheless, the microstructures of laser-annealed sil-

TABLE I. EDX analysis and the estimated thickness of the TiN/Co/Si system with and without PAI after single-pulsed laser annealing at 0.2 *J*/cm^2.

	TiN/Co/PAI/Si		TiN/Co/Si	
	EDX	Estimated thickness (nm)	EDX	Estimated thickness (nm)
Poly-Co	Co:Ti:Si~83:4:13	5	Co:Ti:Si~91:2:7	8.3
Poly-Co silicide	Co:Si~73:27	10	Co:Si~74:26	13
Coarse-grained poly-Co silicide	Co:Si~57:43	12		
a-Si	100	37		

icide layers are different in the two systems. Large and randomly oriented polycrystalline silicide grains are being formed on the amorphized Si substrates, signifying that well intermixing has occurred during the melting and preserved upon fast crystallization. The PAI has played a role in affecting the growth and formation of the Co silicide layer. The amorphized layer has served as the nucleation template for the silicide growth and therefore results in the poly-Co silicide grains, as shown in Fig. 3. It can be further seen from Fig. 3 that the interface between the *a*-Si and the intermixed poly-Co silicide layer is very uniform, abrupt, and sharp, and this can be attributed to the presence of an abrupt melting boundary during annealing since no Co element was detected in the remaining *a*-Si layer. For the non-PAI case, a sharp interface can also be obtained on the crystalline Si, but the melt depth is shallower since the intermixed silicide layer is thinner. This is reasonable as the amorphized Si has a lower melting point (1420 K) compared to *c*-Si,[12,13] and has therefore a larger melt depth. In both systems, the TiN remains intact at low laser fluence of 0.2 J/cm^2.

The microstructures of the TiN/Co/Si system with PAI after single-pulsed laser annealing at 0.7 J/cm^2 are given in Fig. 5. A few layers can be identified from Fig. 5: the top layer is TiN and the bottom layer is a highly textured Co silicide. Figure 5(a) shows that the TiN layer at A is thinner than that at B. This is due to a partial melting of the TiN layer at location A. Besides, a thin residual amorphous Co silicide is being observed just underneath the TiN layer at location A. The bottom poly-Co silicide layer is a highly textured layer with defects oriented in the (111) direction, as shown in high-resolution transmission electron microscopy (HRTEM) of Fig. 5(b). Their corresponding elemental compositions as detected using EDX are shown in Fig. 5(a). The analysis shows only the existence of Co and Si with no detectable nitrogen incorporated in the intermixed silicide layer. An EELS experiment has been carried out to show the Co and Si distributions with some Co-rich intervening regions, as shown in Figs. 6(a) and 6(b).

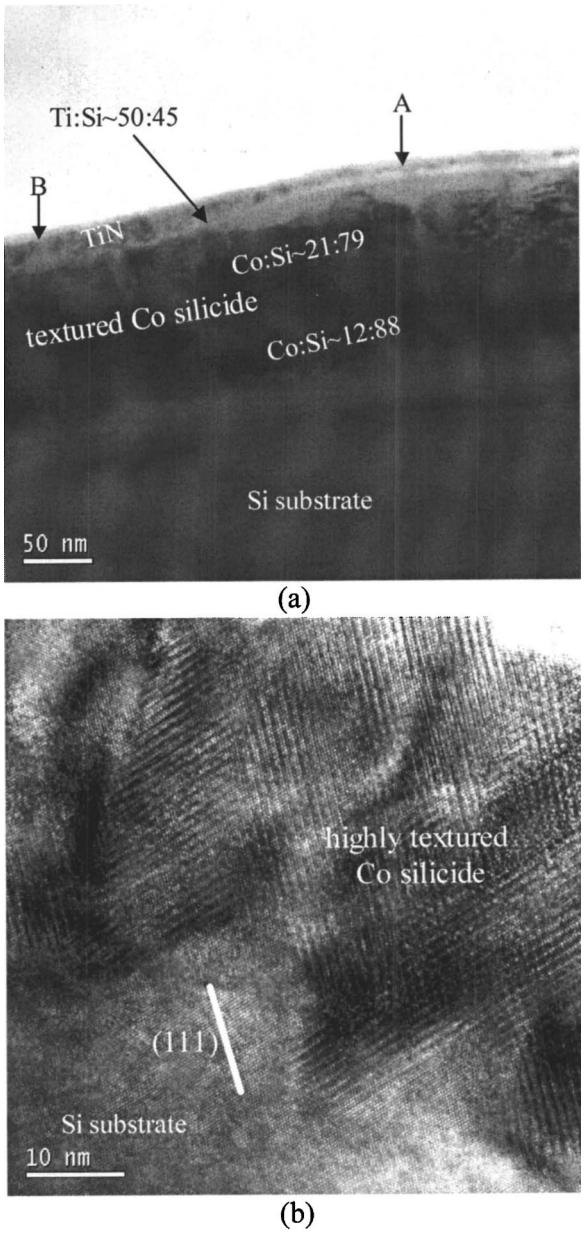

FIG. 5. (a) XTEM and (b) HRTEM images of the TiN/Co/Si system with PAI after single-pulsed laser annealing at 0.7 J/cm^2. The symbols A and B in (a) indicate the location where the TiN capping layer has melted partially and has stayed intact after LTA, respectively. In (b), the highly textured Co silicide grows along the (111) direction of the silicon substrate.

DISCUSSION

Two possible growth mechanisms are proposed for the microstructures formation of Co silicide in the TiN/Co/PAI Si system (as shown in Fig. 3). When a laser pulse is irradiated on the sample, the heat is just enough to partially melt the amorphous Si and some Co at the interface without melting the TiN. This is feasible since the melting temperatures of Co and amorphous Si are 1768 and 1420 K, respectively. During the melting of the *a*-Si layer, some Co atoms partially diffused into the molten phase of Si since the solute atoms prefer to stay in liquid phase than in solid phase.[14] Hence, the interdiffusion and intermix of Co and Si atoms in the liquid phase were resulted. This molten intermix of Co silicide is sandwiched between the nonmelted TiN/Co film stack and partial nonmelted *a*-Si. At the instance of solidification, the contained hot melt of well-intermixed Co and Si may crystallize and propagate from the unreacted Co layer. This is feasible since the top unreacted polycrystalline Co layer could have become the nucleation sites for Co silicide to grow. Simultaneously, another silicide layer nucleates from the liquid/*a*-Si interface using the *a*-Si nuclei as the template. Eventually, the two propagating solid/liquid interfaces collide in the middle; the position where the interfaces meet is the sharp demarcation between the two layers, as shown in Fig. 3.[15]

The second possible growth mechanism for the irradiation of 0.2 J/cm^2 on TiN/Co/PAI Si system can be illustrated in such a way that there is one liquid/solid interface propagating towards the unreacted TiN/Co film stack during the solidification. Comparing the thickness of both layers, the bottom random and larger grain layer is thicker than the top homogeneous layer of poly-Co silicide. Based on the simple expression of heat flow,[16] which is written as

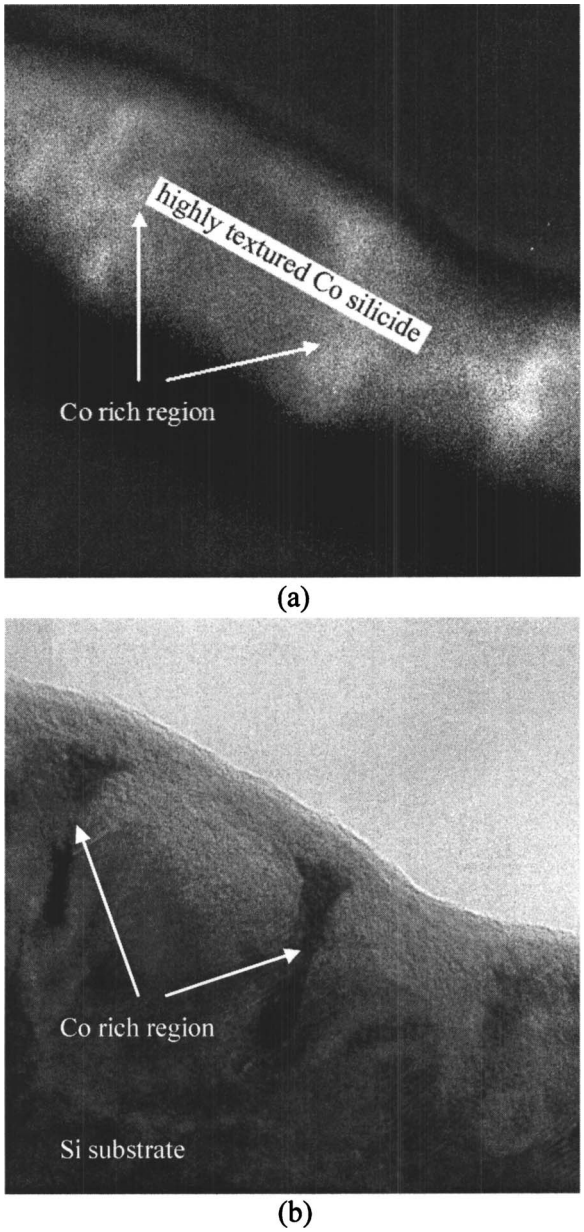

FIG. 6. (a) Elemental mapping of Co of a section of the highly textured CoTi silicide layer. The brighter contrast in the elemental map corresponds to cobalt-rich region. (b) The corresponding XTEM of (a).

$$\Delta H_m \rho v = K \frac{\partial T}{\partial z}, \tag{1}$$

in which ΔH_m is the enthalpy of melting, ρ is the density, v is the velocity of crystallization, K is the thermal conductivity, and $\partial T/\partial z$ is the temperature gradient. During the solidification, the enthalpy of melting must be balanced by the heat flow $K(\partial T/\partial z)$ into the substrate. Initially, the heat-flow gradient available for the heat transport at the liquid/*a*-Si interface is limited by the poor thermal conductivity of *a*-Si.[17] As a result, the initial interface velocity is small. This interface limited crystal growth has given rise to an ample time for recrystallization due to the slow solidification velocity. The structure and phase of the solidified layer are strongly affected by the solidification velocity.[18] Subsequently, the increment in the amount of polycrystalline Co silicide formed enhances the rate of heat transfer from the liquid to the as-grown Co silicide. This is because the as-grown polycrystalline Co silicide possesses better thermal conductivity compared to that of *a*-Si. With the increase of the heat transfer, this has caused the increase in interface velocity according to Eq. (1). When the velocity of solidification front reaches some critical value,[19] the crystallization process takes place without having time for grain growth. Therefore, fine grain of Co silicide having defective and disordered crystallites can be observed on the top of the as-grown coarsed-Co silicide.

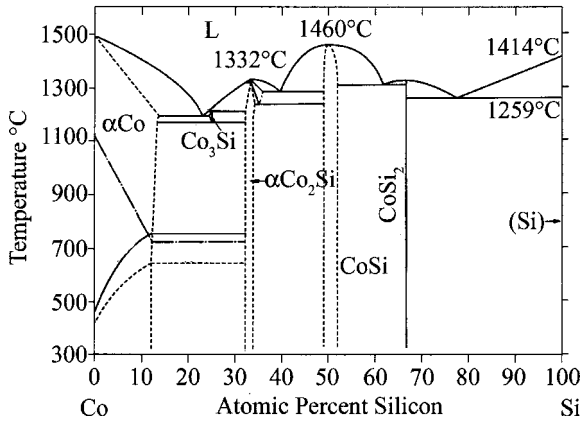

FIG. 7. The phase diagram of Co–Si system (Ref. 21.

For the high fluence of 0.7 J/cm^2 on the TiN/Co/Si system with PAI, the laser energy is high enough to melt the whole Co and PAI layer and it has caused the melt front to propagate beyond the PAI layer as it can be seen from AES shown in Fig. 2(c). Besides, the high fluence has also partially melted the TiN capping layer although TiN has a very high melting temperature. The silicide intermixed layer that is formed is thicker since the melt depth for 0.7 J/cm^2 is larger than 0.2 J/cm^2, as can be seen from the AES. A rough interface of the silicide and substrate [see Fig. 5(b)] can be observed. The interfacial instability can be attributed to the constitutional supercooling (CSC) since it is likely to occur at high fluence.[20] As there is unlimited supply of Si substrate for the reaction with the as-deposited Co layer, large compositional gradients of Co–Si mixture have been resulted after the melting of Co and Si. This concentration gradient of Co and Si atoms in molten phase has led to a gradient of the freezing temperature of the liquid in front of the liquid/solid interface. Based on the two elemental compositions of the textured Co silicide shown in Fig. 5(a), the liquidus temperature of the initial solid/liquid interface (i.e., the interface between the textured Co silicide and the Si substrate) is determined to be lower than the one in the liquid further away from the initial liquid/solid interface. As can be seen from the Co–Si phase diagram[21] in Fig. 7, the liquidus temperature of the more Si-rich Co binary system (i.e., Co:Si~12:88) is higher than the Co–Si binary system which has the composition of Co:Si~21:79. Hence, the liquid in front of the initial liquid/solid interface would have been supercooled. With the compositional gradient of molten phase and the supercooled ahead of the initial liquid/solid interface, this has facilitated CSC. As a result of CSC, precipitated $CoSi_2$

formed between Si grains and cellular structures accompanied by the growth of defects can be observed from the textured Co silicide in XTEM (Fig. 5).[22] The dark contrast of defects that resemble stems and branches can be attributed to twinning, which is generally known as "type-B orientation." It can be seen that defects have grown from the nucleation sites at the silicide/substrate interface and orient in the (111) direction. This phenomenon happens due to the segregation of the Co solute atoms during CSC and later forms along the (111) direction that has the lowest interface energy.[23,24] In addition, the growth of the highly textured Co silicide can be attributed to the epitaxial regrowth with Si substrate as a template. The dark contrast of the textured Co silicide shown in Fig. 5(b) corresponds to Co-rich regions. This has been confirmed by the EELS data (Fig. 6). When the solidification front propagates towards the surface near location A, as shown in Fig. 5(a), the thermodynamic of crystallization has been affected by the presence of Ti.[24] The dissolution of TiN is believed to have led to Ti redistribution and an increase in the Ti concentration in the regions at which the TiN capping layer has partially melted.

CONCLUSION

In summary, the laser-induced reactions of TiN/Co/Si film stacks with and without PAI by irradiation of single pulse excimer laser at low and high fluences have enabled us to identify and understand the transformation of Co silicide microstructure during excimer laser irradiation. The LTA at 0.2 J/cm^2 on the PAI and non-PAI samples has given rise to the formation of different microstructures, in which the understanding of Co silicide growth mechanisms in these two systems has been suggested. The solidification velocity is approximately inversely proportional to the total latent heat liberated at the interface. The LTA at 0.7 J/cm^2 has formed a thick layer of highly textured Co silicide and is attributed to CSC and epitaxial regrowth.

ACKNOWLEDGMENTS

This work was financed in part by Chartered Semiconductor Manufacturing Ltd. and A*STAR Grant No. 0321010007. The authors would like to thank Y. Setiawan, L. Chan, A. Y. Du, K. K. Ong, and Y. F. Chong for their support in this work. One of the authors (F.L.C.) Chow would like to thank Nanyang Technological University for providing a research scholarship.

[1] K. Maex, A. Lauwers, P. Besser, E. Kondoh, M. de Potter, and A. Steegen, IEEE Trans. Electron Devices **46**, 1545 (1999).
[2] D. K. Sohn, J.-S. Park, and J. W. Park, J. Electrochem. Soc. **147**, 373 (2000).
[3] J.-C. Kim, Y.-C. Kim, and H.-I. Seo, IEEE International Symposium on Electronic Materials and Packaging, 19–22 November 2001, Jeju Island, Korea (unpublished), Inspec accession No. 7307173.
[4] R. Lindsay, A. Lauwers, M. de Potter, N. Roelandts, C. Vrancken, and K. Maex, Microelectron. Eng. **55**, 157 (2001).
[5] A. Luches, E. D'Anna, G. Leggieri, and M. R. Perrone, *Laser Technologies In industry* (SPIE, Bellingham, WA, 1988), Vol. 952.
[6] R. A. Roy, C. Cabral Jr., and C. Lavoie, Mater. Res. Soc. Symp. Proc. **564**, 35 (1999).
[7] J.-S. Luo, W.-T. Lin, C. Y. Chang, and W. C. Tsai, J. Appl. Phys. **82**, 3621 (1997).
[8] E. G. Colgan, J. P. Gambino, and Q. Z. Hong, Mater. Sci. Eng., R. **16**, 43 (1996).
[9] P. Liu, C. Hsiao, and C. S. Woo, IEEE Trans. Electron Devices **45**, 1280 (1998).
[10] G. Verma, C. Gelatos, S. Talwar, and J. C. Bravman, IEEE Trans. Electron Devices **49**, 42 (2002).
[11] R. F. Wood and G. E. Giles, Phys. Rev. B **23**, 2923 (1981).
[12] E. P. Donovan, F. Spaepen, D. Turnbull, J. M. Poate, and D. C. Jacobson, Appl. Phys. Lett. **42**, 698 (1983).
[13] M. O. Thompson, G. J. Galvin, J. W. Mayer, P. S. Peercy, J. M. Poate, D. C. Jacobson, A. G. Cullis, and N. G. Chew, Phys. Rev. Lett. **52**, 2360 (1984).
[14] A. Cottrell, *An Introduction to Metallurgy*, 2nd ed. (Edward Arnold, London, 1975).
[15] Y. F. Chong, K. L. Pey, A. T. S. Wee, M. O. Thompson, C. H. Tung, and A. See, Appl. Phys. Lett. **81**, 3786 (2002).
[16] J. M. Poate and James W. Mayer, *Laser Annealing of Semiconductor* (Academic, New York, 1982).
[17] H. Wada and T. Kamijoh, Jpn. J. Appl. Phys., Part 2 **35**, L648 (1996).
[18] P. Baeri, Thin Solid Films **241**, 141 (1994).
[19] R. F. Wood and G. A. Geist, Phys. Rev. B 31, 2606 (1986).
[20] J. S. Luo, W. T. Lin, C. Y. Chang, P. S. Shih, and F. M. Pan, J. Vac. Sci. Technol. A **18**, 143 (1999).
[21] T. B. Massalski, *Binary Alloy Phase Diagrams* (American Society for Metals, Metal Park, OH, 1986).
[22] R. T. Tung, J. M. Gibson, D. C. Jacobson, and J. M. Poate, Appl. Phys. Lett. **43**, 476 (1983).
[23] D. P. Adams, S. M. Yalisove, and D. J. Eaglesham, J. Appl. Phys. **76**, 5190 (1994).
[24] F. L. Chow, K. L. Pey, P. S. Lee, C. H. Tung, X. C. Wang, G. C. Lim, and Y. F. Chong, Electrochem. Solid-State Lett. **7**, G213 (2004).